Master's Thesis

석사 학위논문

Layer-by-layer control of black phosphorene-metal contact ; Schottky barrier and carrier polarity

Su Yeong Lee (이 수 영 李 秀 英)

Department of Emerging Materials Science

신물질과학전공

DGIST

2016

Master's Thesis

석사 학위논문

Layer-by-layer control of black phosphorene-metal contact ; Schottky barrier and carrier polarity

Su Yeong Lee (이 수 영 李 秀 英)

Department of Emerging Materials Science

신물질과학전공

DGIST

2016

Layer-by-layer control of black phosphorene-metal contact
; Schottky barrier and carrier polarity

Advisor : Professor 이재동

Co-advisor : Professor 이종수

by

Su-Yeong Lee

Department of Emerging Materials Science

DGIST

A thesis submitted to the faculty of DGIST in partial fulfillment of the requirements for the degree of Master of Science in the Department of Department of Emerging Materials Science. The study was conducted in accordance with Code of Research Ethics[1)].

05. 30. 2016

Approved by

Professor 이 재 동 (Signature)

(Advisor)

Professor 이 종 수 (Signature)

(Co-Advisor)

Declaration of Ethical Conduct in Research**:** I, as a graduate student of DGIST, hereby declare that I have not committed any acts that may damage the credibility of my research. These include, but are not limited to: falsification, thesis written by someone else, distortion of research findings or plagiarism. I affirm that my thesis contains honest conclusions based on my own careful research under the guidance of my thesis advisor.

Layer-by-layer control of black phosphorene-metal contact
; Schottky barrier and carrier polarity

Su-Yeong Lee

Accepted in partial fulfillment of the requirements for the degree of Master of Science.

05. 30. 2016

Head of Committee _____(인)

Prof. 이 재 동

Committee Member _____(인)

Prof. 이 종 수

Committee Member _____(인)

Prof. 정 낙 천

MS/EM
201421003

이 수 영. Su-Yeong Lee. Layer-by-layer control of black phosphorene-metal contact; Schottky barrier and carrier polarity. Department of Emerging materials Scienge. 2016. p.38. Advisors Prof. J. D. Lee. Prof. Co-Advisors Jong-Soo Lee.

Abstract

Layered black phosphorus (BP) attracts great attention as promising candidates for the nanoelectronics and the field-effect transistor (FET) due to their excellent mechanical, optical, thermoelectric, and electronic properties. For a practical device realization, it is important to control electronic transport properties and contact resistance at the interfaces between semiconducting BP and metal electrode. In this work, based on the state-of-the-art band unfolding technique combined with the first-principles calculation, we identify the band structure of BP layer by layer and tune the Schottky barrier height and control the carrier-type of the BP-metal contact.

Keywords : black phosphorus , Density functional theory, Schottky barrier, contact resistance

CONTENTS

LIST OF TABLES & FIGURES

1. INTRODUCTION

Black phosphorus [1,2,3], the most stable form of all the phosphorus allotropes, is a layered two-dimensional material in which each phosphorus atom is covalently bonded with three adjacent phosphorus atoms to form a puckered honeycomb structure and individual atomic layers are stacked together by Van der Waals interactions (as illustrated in Figs. 1a (top-view) and 1b (side-view)). Most recently, it attracts great attention as promising candidates for the nanoelectronics and the field-effect transistor (FET) [4,5,6,7] due to many unique properties not found in other members of the 2D materials family such as its high carrier mobility, which is up to 1000 $cm^2V^{-1}s^{-1}$ at room temperature [8,9,10], and thickness-dependent direct band gap with a predicted band gap that change considerably as a function of the number of layers, varying from 2 eV to 0.3 eV [11,12,13,14,15]. Such a band structure and the thickness-dependent direct band gap, (as shown in Fig. 2) may lead to potential applications. For a practical device realization, it is essential to get a detailed understanding of contact between metals and BP. The major issue for the fabrication of FET transistor is existence of a contact resistance at the interface between the 2D semiconductor and metal because of low contact resistance that have a significant impact on the overall efficiency of the device [16,17]. In order to achieve high performance of the device, the low contact resistance of the metal contact interface in the fabrication of an electronic device is a key because it is necessary to reduce power loss and to improve electron or hole injection efficiency across the metal/semiconductor interface. One of main factors that determine such a contact resistance in the device is Schottky barrier which is a critical parameter [18,19,20].

When the charge transfers from the semiconductor to the metal, it needs to overcome the Schottky barrier at the semiconductor/metal interface [21-24]. Therefore, lowering the

Schottky barrier height (SBH) is of great importance and it is essential to get a detailed understanding of the Schottky barrier height between BP and metals [7,25,26] for the fabrication of electronic devices.

Generally, SBH is determined by Schottky-Mott rule [4,27]. According to Schottky-mott rule, electron and hole Schottky barrier heights should depend on vacuum work function of metal which is relative to the electron affinity of the semiconductor. However, in practice, it was found experimentally that predicted SBH is a less sensitive function of the metal work function and may be almost independent of the choice of metal because Fermi level pinning likely occurs at the contacts. (Fermi-level pinning effect) [28,29]. Base on the Fermi level pinning behavior at the metal/semiconductor interface, an n-type Schottky barrier Φ_{Bn} is defined the energy difference between the Fermi level E_{F} and the conduction band minimum E_C ($\Phi_{Bn} = E_C\text{-}E_F$). Similarly, a p-type Schottky barrier Φ_{Bp} is defined the energy difference between the Fermi level E_{F} and valence band maximum E_V ($\Phi_{\mathrm{Bp}} = E_F\text{-}E_V$) [21,22,30,31].

Moreover, the sum of two types of Schottky barriers (n- and p-type) is approximately equal to the band gap value E_G ($\Phi_{\mathrm{Bn}} + \Phi_{\mathrm{Bp}} \approx E_G$). In view of the above, we have performed the first-principles calculations to predict the SBH, which provides the fundamental understanding of the BP-metal interfacial. Schottky barrier height is estimated along with fundamental understanding of the interfacial atomic and electronic structure calculation, which ultimately determine the barrier. We have studied interfacial properties of BP on several commonly used metal (Ti, Sc, Al) varying thickness of BP as stacking layer number of few-layer phosphorene from 1L to 4L. Our calculation points out the fact that the carrier type and Schottky barrier height is strongly dependent on BP layer number. While a number of studies have been carried out to understand the interfacial and electronic properties of monolayer or bilayer phosphorene-metal contact, how to control carrier type and tune the

SHB in the metal/BP contact under different thickness of BP has not been systematically and comprehensively studied so far. Therefore, our results show a switching mechanism at the BP/metal interface that depends on both the contact metal and layer thickness of BP plays a crucial role in changing the Schottky barrier height formed at BP/metal interface.

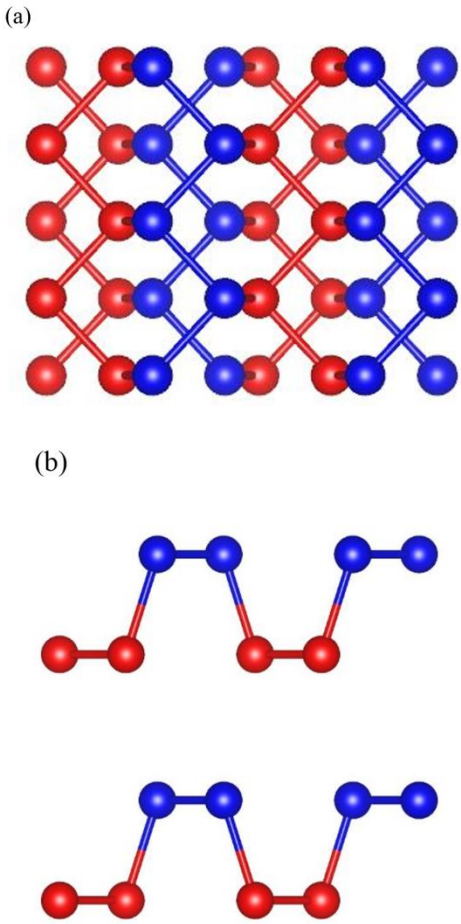

Figure 1. The ball-stick model of few-layer phosphorus. (a) Top and (b) side view of bilayer Phosphorene.

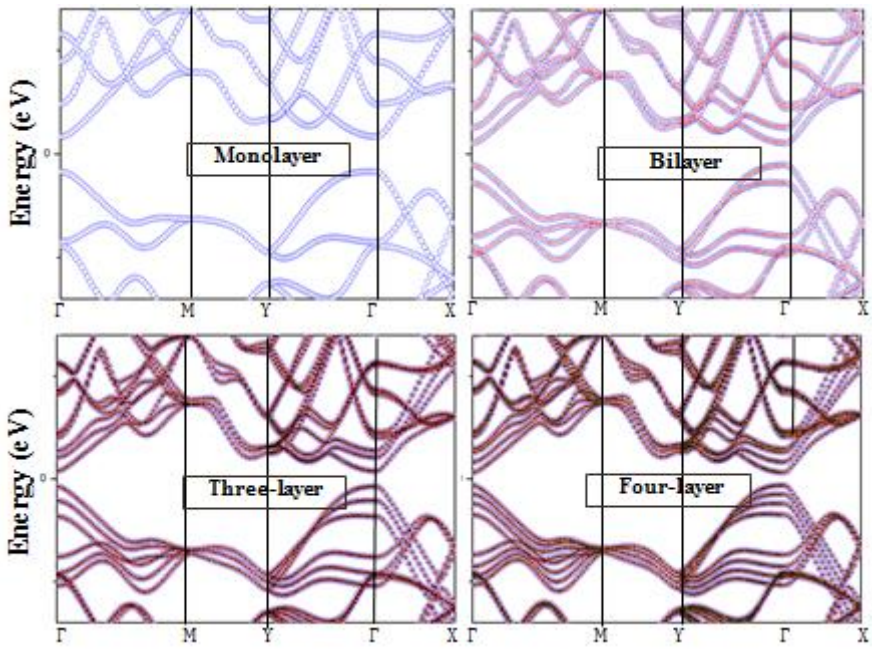

Figure 2. The DFT calculated band structure of Black phosphorene according to the stacking layer number of few-layer phosphorene

I. METHOD

1.1 Density-functional theory

Density functional theory is an approach for the description of ground state properties of matter laying emphasis on the charge density. The main idea of DFT is to determine the properties of a many-electron system by using its electron density and not via its many-body wave function. Moving from E[ψ] to E[ρ] significantly reduces the computational effort needed to understand electronic properties of atoms, molecules, and solids. For these reason, the density functional theory (DFT) is presently the most successful approach for computations of the quantum state of atoms, molecules, and the condensed matter systems.

2.2 Hohenberg-Kohn theorem

In 1964, Hohenberg and Kohn [32] first derived the fundamentals of density-functional theory which allows to express all ground-state properties as a functional of electron density n(r). The first Hohenberg-Kohn theorem asserts a one-to-one correspondence that the density of any system determines all ground-state properties of the system. According to the first Hohenberg-Kohn theory, if the system has a nondegenerate ground state, it means that there is only one ground-state charge density ρ(r) that corresponds to a given V (r). By proving contradictions, we can verify the first Hohenberg-Kohn theorem. Many-electron Hamiltonian with ground state wavefunction Ψ is given by

$$H = T + U + V \quad , \quad (1)$$

where T means the kinetic energy and U and V the electron-electron interaction.

If we consider that there is two distinct external potential $v_1(r)$ and $v_2(r)$, we will have two different Hamiltonians H and H' whose ground state electron density is the same but the normalized wave function ψ and ψ' would be different, can be stated as following:

$$E_0 < \langle\psi'|\mathrm{H}|\psi'\rangle = \langle\psi'|\mathrm{H}'|\psi'\rangle + \langle\psi'|\mathrm{H}-\mathrm{H}'|\psi'\rangle = \mathrm{E_0}' + \int \rho(r)[v(r)-v'(r)]dr \quad (2)$$

$$E'_0 < \langle\psi|\mathrm{H}'|\psi\rangle = \langle\psi\,|\,\mathrm{H}\,|\,\psi\rangle + \langle\psi|\mathrm{H}'-\mathrm{H}|\psi\rangle = \mathrm{E_0} - \int \rho(r)[v(r)-v'(r)]dr \quad (3)$$

When we add the two equations (2) and (3), we then obtain the following interaction formula

$$E_0 + E'_0 < \mathrm{E_0}' + \mathrm{E_0}$$

Since two equations contradict each other, there are no two different external potentials that can give the same ρ(r). Thus ρ(r) uniquely determines *v(r)* (to within a constant) and all ground-state properties.

Thus the energy functional can be represented by

$$E_v[\rho] = \langle\psi[\rho]|\widehat{H}|\psi[\rho]\rangle = \langle\psi[\rho]|\widehat{T}+\widehat{U}|\psi[\rho]\rangle + \langle\psi[\rho]|\widehat{V}|\psi[\rho]\rangle \ , \quad (4)$$

$$E_v[\rho] = F_{HK}[\rho] + \int \rho(r)v(r)dr, \quad (5)$$

where $F_{HK}[\rho] = G[\rho] + \frac{1}{2}\int \frac{\rho(r)\rho(r')}{|r-r'|}drdr'$(6) includes coulomb energy term and unknown term G[ρ]. Here note that $F_{HK}[\rho]$ is only dependent on ρ (r) and independent of any external potential v(r). Since the total energy is a universal functional of the electron density, one can apply the variational principle to minimize the energy with respect to the electron density.

$$E_0[\rho_0] \leq E_v[\rho] \quad (7)$$

Therefore, the exact ground-state density can be decided by minimum value of $E_v[\rho]$.

2.3 Kohn-Sham equations

In 1965, Kohn and Sham published Kohn and Sham theorem [53] which transformed density-functional theory into a practical electronic structure theory. According this theorem, the real system of interacting electrons is mapped on to a fictitious system of non-interacting electrons where ground-state density having the same ground state charge density ρ (r). In other words, real and fictitious system have the same positions and atomic numbers of the nuclei (same density).

In Eq.8, Kohn-Sham write the unknown term G[ρ] in the following form

$$G[\rho]=T_s[\rho] + E_{xc}[\rho] \ , \quad (8)$$

which consists of kinetic energy of non-interacting electrons (T_s) and all the many-body quantum effects are put into the exchange and correlation energy (E_{xc}). From Eq (6) to (8) the HK variational principle for interaction electrons is rewritten as the follow energy functional.

$$E_{KS}\ [\rho] = T_s[\rho(r)] + \frac{1}{2}\int \frac{\rho(r)\rho(r')}{|r-r'|} dr dr' + E_{xc}[\rho(r)] + \int \rho(r) v(r) dr \quad (9)$$

We can write down Hamiltonian operator in terms of some functional derivatives, which means potentials.

$$\left(-\frac{\hbar}{2m}\nabla^2 + V(r) + V_H(r) + V_{XC}(r)\right)\psi_i(r) = \varepsilon_i \psi_i(r) \ , \quad (10)$$

where we have introduced a Hartree potential

$$V_H(r) = e^2 \int \frac{\rho(r')}{|r-r'|} dr' \quad (11)$$

and an exchange-correlation potential

$$V_{XC}(r) = \frac{\delta E_{xc}[\rho(r)]}{\delta \rho(r)} \ . \quad (12)$$

In these functional derivatives, the exchange-correlation energy $E_{xc}[\rho(r)]$ and potential are still unknown. Therefore, we can calculate Schrödinger equation just by approximating exchange-correlation potential in order to express functional type of electron density. There are many kinds of functionals used. All of them, Local-Density Approximation (LDA) and Generalized Gradient Approximation (GGA) are the most common and well-known functionals in these days.

2.4 Exchange correlation functionals

For practical use of the Kohn-Sham equations**,** we have to know what the form of the exchange-correlation energy functional is. The most widely used and most simple approximation for E_{xc} is the local density approximation which uses the electron density under a uniform and locally homogeneous electron gas environment.

2.4.1 The local-density approximation (LDA):

A class of the approximations to the exchange-correlation (XC) energy functional in density functional theory (DFT) is the LDA [34-36], which assumes that the exchange-correlation energy at a point **r** is simply equal to the exchange-correlation energy of a uniform electron gas that has the same density at the point **r**. The exchange correlation energy for the density within each volume is then assumed to be the exchange correlation energy obtained from the uniform electron gas for that density.

Thus the total exchange-correlation energy of the system can be written in the following form:

$$E_{XC}^{LDA}[\rho(r)] \equiv \int \rho(r)\varepsilon_{XC}^{hom}[\rho(r)]dr \ , \quad (13)$$

where ε_{XC}^{hom} represents the exchange-correlation energy per particle of a homogeneous gas of electrons of density $[\rho(r)]$. The density $[\rho(r)]$ as usual, represents the number of electrons per unit volume. So that the exchange-correlation potential $V_{XC}(r)$ may be written

$$\mathrm{V}_{XC}(r) = \frac{\delta E_{XC}[\rho(r)]}{\delta\rho(r)} = \varepsilon_{XC}[\rho(r)] + \rho(r)\frac{d\varepsilon_{XC}(n)}{dn}\Big|_{n=\rho(r)} . \ (14)$$

Despite the simple, the LDA results in a realistic description of the atomic structure, elastic, and vibrational properties for a wide range of systems. But, it only can be used in the space where electron densities slowly varying. The uniform electron gas isn't such a great model in molecules because the electron density can vary rapidly over a small region of space. One way to improve is to make the functional depend on both the density and the gradient of the density.

2.4.2 Generalized gradient approximation (GGA):

The accuracy of LDA is often satisfied in condensed-matter systems, but it is much less in atomic and molecular physics. Such problems are mostly corrected by the introduction of gradient corrections. These depend not only on the value of the density at a point but also on its gradient. So, the GGA (generalized gradient approximation) [37-39] XC functional can be written as

$$E_{XC}^{GGA}[\rho(r)] = \int \rho(r)\varepsilon_{XC}[\rho(r), \nabla\rho(r)]dr \ . \ (15)$$

Many GGA functionals have been proposed. Some of the most widely used one are Perdew-Wang 91 (PW91) and Perdew-Burke-Ernzerhof (PBE) [40,41,42].

2.5 Reciprocal space

Many physical properties of crystals as well as the geometry of the 3D patterns resulting from a diffraction event are most easily represented using the concept of the reciprocal lattice. Thus we must understand the lattice of materials to understand many physical properties [43]. If a, b, and c are the primitive vectors of the direct lattice and a direct lattice vector $\vec{r}$ defined as

$$\vec{r} = u\vec{a} + v\vec{b} + w\vec{c} \qquad (16)$$

Then the reciprocal lattice is described by the corresponding primitive vectors

$$\vec{a}^* = 2\pi \frac{\vec{b}\times\vec{c}}{\vec{a}\cdot(\vec{b}\times\vec{c})} = 2\pi \frac{\vec{b}\times\vec{c}}{V} \ , \qquad (17)$$

$$\vec{b}^* = 2\pi \frac{\vec{c}\times\vec{a}}{\vec{a}\cdot(\vec{b}\times\vec{c})} = 2\pi \frac{\vec{c}\times\vec{a}}{V} \ , \qquad (18)$$

$$\vec{c}^* = 2\pi \frac{\vec{a}\times\vec{b}}{\vec{a}\cdot(\vec{b}\times\vec{c})} = 2\pi \frac{\vec{a}\times\vec{b}}{V} \ . \qquad (19)$$

Here, $a_1 \cdot (a_2 \times a_3)$ is a volume of single lattice unit cell. By using properties of the dot product, we can understand the relationship of the reciprocal lattice axis vector and direct lattice axis vector.

$$\vec{a}^* \cdot \vec{b} = \frac{\vec{b}\times\vec{c}}{V} \cdot \vec{b} = 0 \qquad (20)$$

$$\vec{a}^* \cdot \vec{c} = \frac{\vec{b}\times\vec{c}}{V} \cdot \vec{c} = 0 \qquad (21)$$

From these equations, we can understand that reciprocal lattice axis vector $\vec{a}^*$ is perpendicular to the direct lattice axis vector $\vec{b}$ and $\vec{c}$ plane in real space which is the

reciprocal lattice vector for a.

$$\vec{a}^* \perp bc \qquad (22)$$

In the same manner,

$$\vec{b}^* \cdot \vec{c} = \vec{b}^* \cdot \vec{a} = 0 \qquad (23)$$

$$\vec{c}^* \cdot \vec{a} = \vec{c}^* \cdot \vec{b} = 0 \qquad (24)$$

The reciprocal lattice axis vector $\vec{b}^*$ is perpendicular to the direct lattice axis vector $\vec{c}$ and $\vec{a}$ and $\vec{c}^*$ are perpendicular to the direct lattice axis vector $\vec{a}$ and $\vec{b}$.

$$\vec{b}^* \perp ca \quad (25)$$

$$\vec{c}^* \perp ab \quad (26)$$

Using the relations between direct and reciprocal lattice it can be shown that the reciprocal lattice of *sc* is *sc* (at **k** space), the reciprocal of *bcc* is *fcc*, and reciprocal of *fcc* is *bcc*.

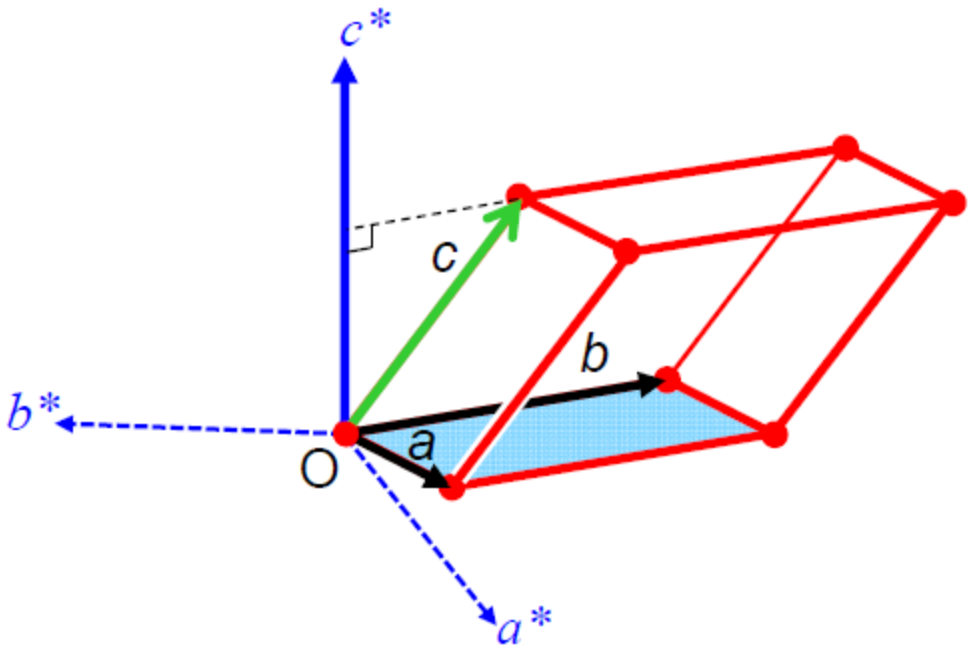

Figure 3. Diagam of relation between reciprocal and real space vector

2.6 Brillouin zone

A Brillouin Zone [44] is defined as a Wigner-Seitz primitive cell in the reciprocal lattice. The first Brillouin zone is defined to be the Wigner-Seitz primitive cell of the reciprocal lattice, or it could be defined as the set of points in **k** space that can be reached from the origin without crossing any Bragg plane. In other words, the first Brillouin zone is a geometrical construction to the WS primitive cell in the k-space. To construct the WS primitive cell in the k-space, draw lines to connect a given lattice points to all nearby lattice points and then draw new lines or plane at the mid point and normal to the lines. The smallest volume enclosed in this way is the WS primitive cell.

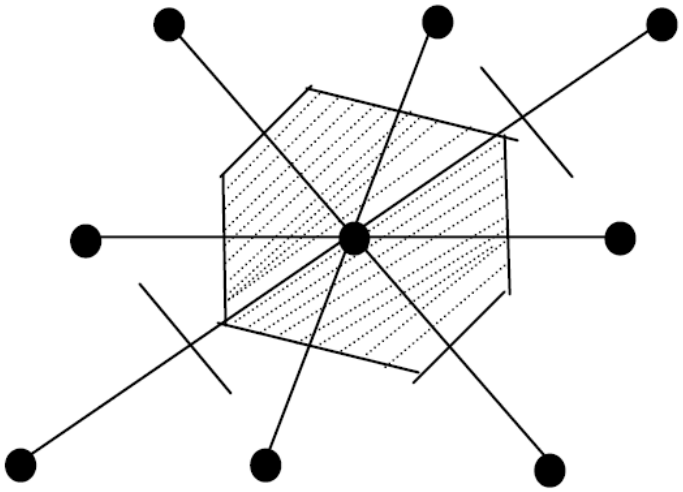

Figure 4. How to draw the first Brillouin zone

The second Brillouin zone is the set of points that can be reached from the first zone by crossing only one Bragg plane. The (n + 1)th Brillouin zone is the set of points not in the (n - 1)th zone that can be reached from the nth zone by crossing n - 1 Bragg planes. Since many properties including electronic property of material can be understood by Brillouin zone, it is definitely important in studying various materials.

2.7 Unfolding band technique (BandUP)

When a large “super cell” is involved, general DFT calculations are impossible to calculate band structure of supercell. Then the period of the super cell grows longer, the corresponding first Brillouin zone of the super cell (SBZ) shrinks its size. In turn, bands in the first Brillouin zone of the normal cell (NBZ) get “folded” into the SBZ as illustrated in Fig.5

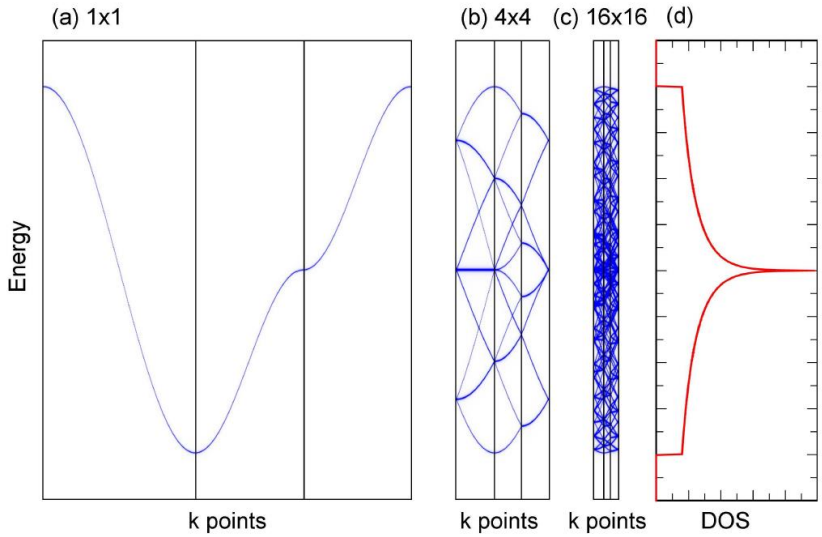

Figure 5. Illustration of band folding in the supercell calculations: (a) band structure of a two-dimensional one-band first-neighbor tight-binding model, (b) the same obtained from a 4×4 supercell calculation, and (c) the same obtained from a 16×16 supercell calculation.

BandUP [45-47] is a code that allows you to obtain a primitive cell representation of the band structure of systems simulated using supercells. The band unfolding technique is to recover an effective primitive cell. One can obtain a primitive cell representation of band structures calculated using supercells.

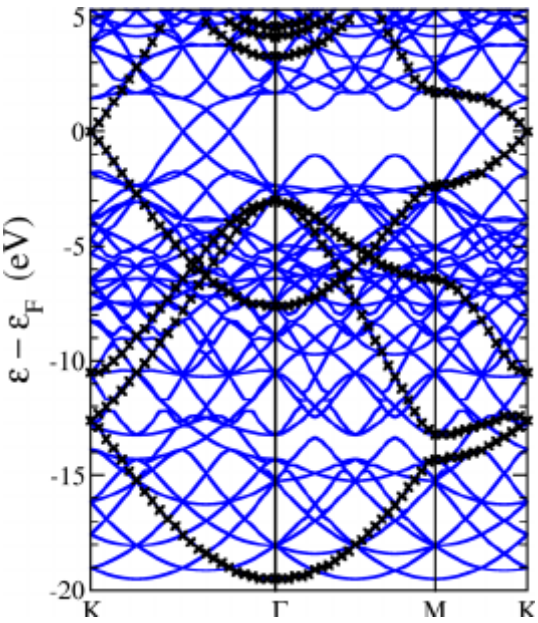

Figure 6. Band structure for a 4 × 4 supercell of graphene, before (blue lines) and after (black lines) unfolding.

II. Calculation details

Our calculations were all carried out using density functional theory (DFT) as implemented in the Vienna initio simulation package (VASP) [48]. Core and valence electrons were treated using the projector-augmented wave pseudopotentials while electron exchange and correlation was treated using the Perdew-Burke-Ernzerhof (PBE) form of the generalized gradient approximation [49-51]. The plane wave kinetic energy cutoff is set at 400eV. The metal substrates were modeled by slab of 4 atomic layers and the BP-metals systems were modeled by placing the BP on top of the metal surfaces. A vacuum region more than 12Å in the z-direction was used to ensure decoupling between neighboring slabs. During structural relaxation, only the bottom two layers of metal atoms were fixed in their respective bulk positions, with all the other atoms fully relaxed until all force on any given atom is less than 0.001eV/ Å. In order to simulate the BP/metal vdW heterostructures, we choose two different lattice structures and lattice constants, which make them have a lattice mismatch for each other.

The lattice constants of the metals and BP were obtained via structural optimization. Calculated lattice parameters for the BP are a =4.58Å, b=3.305 Å respectively. Optimized lattice parameters for metals are a =2.858 Å, b=4.950 Å for Al (111), a=5.733 Å, b=3,310 Å for Sc (0001), and a=2.951 Å, b=5.111 Å for Ti (0001). Due to the lattice mismatch between BP and metal, supercell calculation is performed. All supercells in this paper are chosen in order to minimize the impact of lattice mismatch [52], as listed in Fig. 7. In addition, the lattice mismatch in each metal is listed in Fig. 7, ranging from 0.1%–4.0%. BP/Al heterostructures by combining a (3 × 3) supercell of BP (001) and a (5 × 2) supercell

of Al metal (111) lead to a lattice mismatch of 4.0%, 0.1% along *x*-axis and *y*-axis respectively. BP/Sc heterostructures by combining a (5 × 1) supercell of BP (001) and a (4 × 1) supercell of Sc metal (0001) lead to a small lattice mismatch of 0.4%, 0.9%, along *x*-axis and *y*-axis respectively. BP/Ti heterostructures are composed of a supercell (4 × 3) of BP (001) and a (3 × 2) supercell of BP (0001), where have a lattice mismatch of 2.3% and 3.8%, along *x*-axis and *y*-axis respectively. All of the models are shown in Table1.

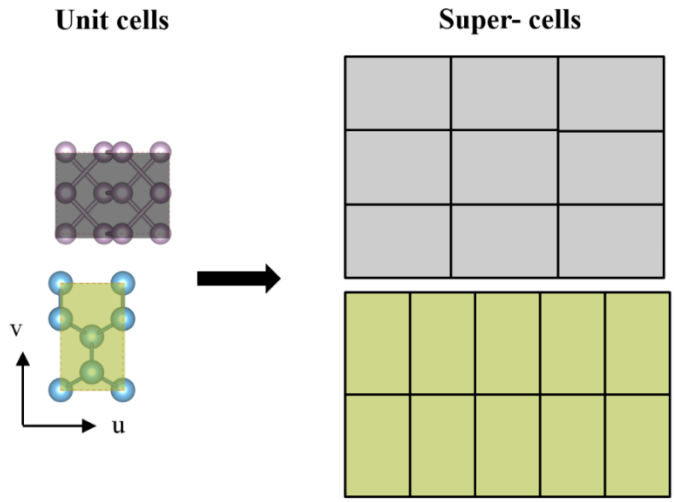

Interface	BP(u×v)	metal(u×v)	mismatch(u,v)	
BP/Al (111)	3 × 3	5 × 2	4.0%	0.1%
BP/Sc (0001)	5 × 1	4 × 1	0.4%	0.9%
BP/Ti (0001)	4 × 3	3 × 2	2.3%	3.8%

Figure 7. The use of supercells to overcome lattice mismatch. Details of metal orientation, the supercells and mismatch used in this paper are given.

For these cells, we use a Monkhorst-Pack [49] grid of k-point 8 × 8 × 1 mesh for BP/Ti , 7 × 10 × 1 for BP/Al and 1 ×8 ×1 for BP/Sc depending on the cell size. When the period of the supercell grows longer, the corresponding first Brillouin zone of the supercell shrinks its size. But the effective primitive cell is recovered by using the band unfolding technique (BandUP) [46]. That is, we use a modified effective band structure (EBS) technique to unfold bands from supercell calculations using our implementation, based on the method by Popescu and Zunger to directly observe the band structure of BP/metal contact.

III. RESULT AND DISCUSSION

3.1 BP/Ti contact system

We first investigated the thickness dependence of charge transport between BP and Ti metal substrate. Figure 9 shows that the interfacial properties of layer by layer deposition of BP on Ti substrate. We use four layers of Ti metal atoms in (0001) orientation to model the metal surface and place the BP on top of the metal surface. The most stable BP/Ti metal contact geometries are obtained by optimizing the structure from different initial configurations of BP-Ti systems. The side view and top views of the optimized most stable geometry are illustrated in figure 8. (a) and (b). As shown in Figure 8. (a) and (b), the original structure of layer of BP which is nearest to metal surface is distorted seriously on Ti metal electrode, suggestive of a strong interaction between phosphorus and metal surface. Our overall calculated band structures of the BP-Ti contact system under different layer number of BP increased from 1 to 4 are shown in Figure 9(a)-(d). In overall band structure, the Fermi level is pinned between VBM and CBM. As mentioned above, the Schottky barrier Φ_{SB} is predicted by the energy difference between E_F of the interfacial system and the CBM (n-type) or VBM (p-type) of BP. That is, the n-type Schottky barrier height is defined as Φ_{Bn}= E_C-E_F, where E_C is the conduction band minimum (CBM), and E_F represents the Fermi level. Likewise, a p-type Schottky barrier height is given by Φ_{Bp}= E_F-E_V, where E_V is the valence band maximum (VBM). In a monolayer phosphorene-metal system (Fig 9. (a)), we can't predict Φ_{SB} because original structure of the nearest BP layer to metal substrates is destroyed seriously as you see Fig. 8(b) and it suggests that it loses nature properties of BP and changes other system. Therefore, we do not regard the nearest BP layer to metal as a BP. In Fig. 9(b), the Fermi level is located between the conduction and valence bands and is

closer to the CBM, where the n-type Schottky barrier forms. The n-type Schottky barrier height of Φ_{Bn} = 0.4 eV appears. In Fig. 9(c), we newly propose method to predict Φ_{Bn} and Φ_{Bp} in multilayer. As shown in Figure 9(c), the numbers of energy bands are doubled when another layer is put a bilayer BP, and the obvious band splitting can be seen from figure 9(c). Relative Three-layer BP-metal system, the increase of the band splitting in four-layer BP-metal can be seen from Figure 9(d) too.

Splitted bands are originated from each layer at multilayer of BP-metal system and it played a key role in SBH since each layer have effect on transport of charge when charges inject from metal to BP. We have regarded every SBH derived from each layer, then averaged every SBH. When applied at Γ point in Figure 8(c), the splitting of VB is 0.83eV. We averaged energy difference between E_F and CB of each splitting bands which are 0.24 eV and 1.07 eV and averaged value is 0.655 eV. Therefore, the CBM of three-layer BP-metal are closer to the Fermi levels than the VBM, leading to the *n*-type contact. The n-type Schottky barrier height of Φ_{Bn} = 0.39eV appears. In Fig. 9(d), we averaged energy difference between E_F and CB or VB of each splitting band in like above manner. Energy difference between E_F and splitting band of VB are 0.08, 0.65, 1.25 eV respectively and averaged value is 0.66 eV. Thus, the CBM of 4L BP-metal are closer to the Fermi levels than the VBM, leading to the *n*-type contact. The n-type Schottky barrier height of Φ_{Bn} =0.28 eV appears. It is shown that the SBH becomes smaller and smaller with layer number increase.

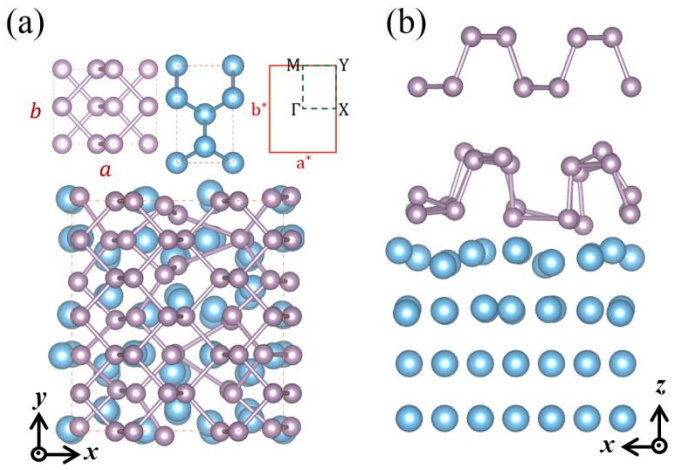

Figure 8. Interfacial structures of the most stable configuration for BP on metal surfaces.

(a)Top views and (b) side view of double layer of BP on the Ti (0001) surface.

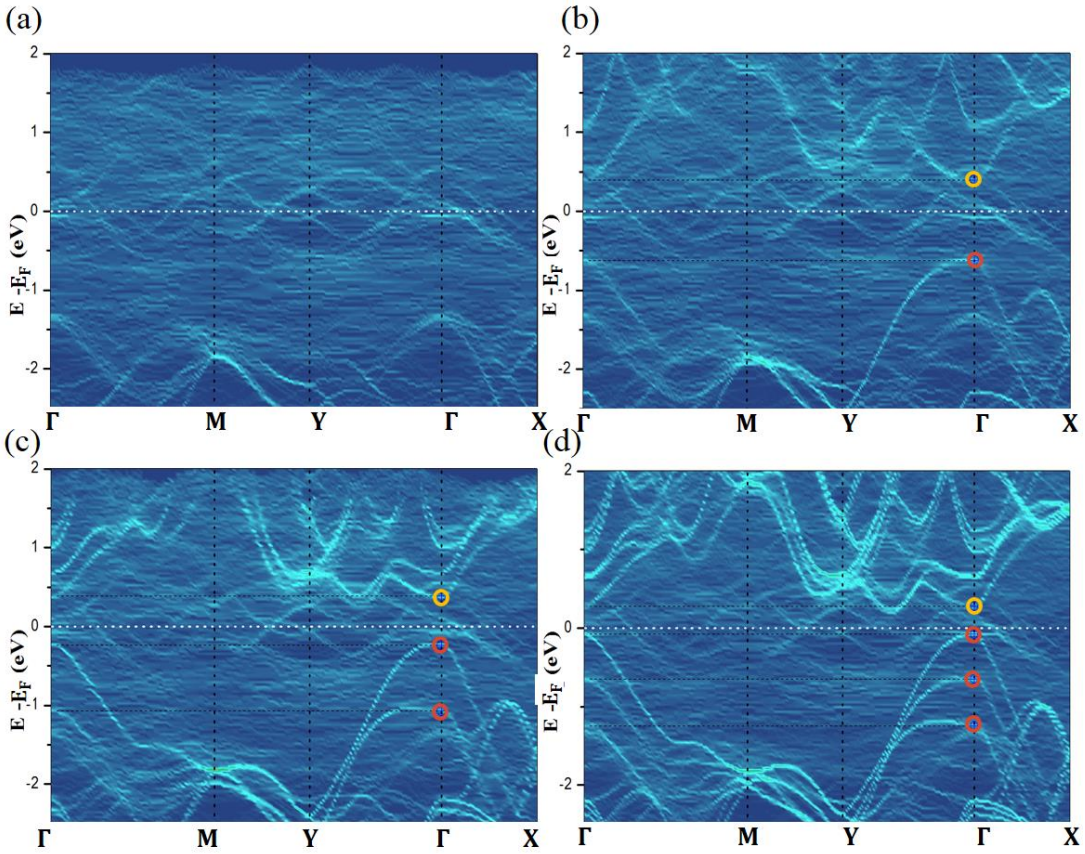

Figure 9. Calculated interfacial properties of BP on the metal surfaces. The unfolding band structure projected contributions from the wave function on the BP orbitals. The line width is proportional to the weight. The Fermi level is set at zero.

3.2 BP/Sc contact system

We next investigated the thickness dependence of charge transport with BP/Sc contacts. Our overall calculated band structures of the BP-Sc contact system under different layer number of BP increased from 1 to 4 are shown in Figure 11 (a)-(d). The Schottky barrier Φ_{SB} is predicted by the energy difference between E_F of the interfacial system and the CBM (*n*-type) or VBM (p-type). In common of a monolayer phosphorene-Ti system case, we can't predict SBH of 1L BP/Sc metal contact by the same token. In Fig. 11(b), the Fermi level is located between the conduction and valence bands and energy difference between E_F of the interfacial system and the CBM (*n*-type) is approximately equal to VBM (p-type), leading ambipolar behavior. The n - and p - type Schottky barrier height of Φ_{Bn} = 0.55 eV and 0.5 eV appear, respectively. In Figure 11(c), Energy difference between E_F and splitting band of VB are 0.37, 1.0, respectively and averaged value is 0.685 eV. Energy difference between E_F and CBM is 0.5 eV. The Fermi level is located between the conduction and valence bands and is closer to the CBM, where the n-type Schottky barrier height of Φ_{Bn} = 0.5 eV appears. In Figure 11(d), Energy difference between E_F and splitting band of VB are 0.1, 0.72 and 1.21eV respectively and averaged value is 0.66 eV. Energy difference between E_F and CBM is 0.39 eV. Since the Fermi level of combined system lies between CBM and VBM and the CBM is closer to the Fermi level than the VBM, an n-type Schottky barrier (Φ_{Bn}) forms. The n-type Schottky barrier height of Φ_{Bn} = 0.39 eV appears. BP transistors with Sc contacts demonstrate ambipolar behavior is switched to n-type behavior, as can be seen in Figure 11. (b) and Figure 11. (d). This equipped with the ability to switch between ambipolar and n-type conduction through the control of thickness that is likely Layer by layer control.

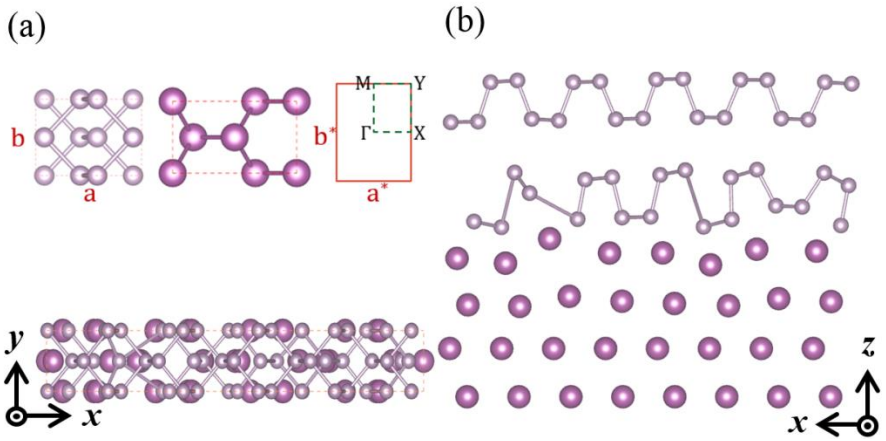

Figure 10. Calculated Interfacial structures of the most stable configuration for BP on Sc metal surfaces. (a)Top views and (b) side view of double layer of BP on the Sc (0001) surface.

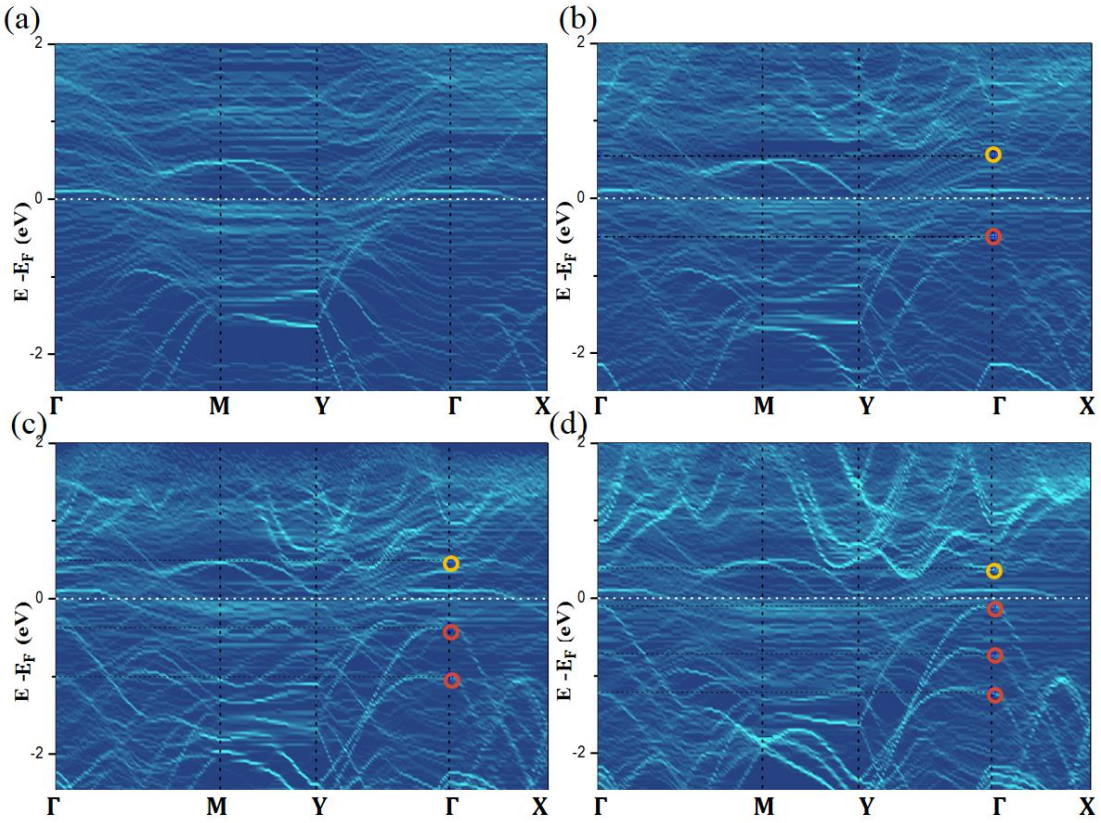

Figure 11. Calculated interfacial properties of BP on the Sc metal surfaces. The unfolding band structure projected contributions from the wave function on the BP orbitals. The line width is proportional to the weight. The Fermi level is set at zero.

4.3 BP/Al contact

For Al contacts, the obtained Φ_{SB} by band structure is presented listed in Fig. 13 (a) – (d). As shown in Figure 12. (a) and (b), the original structure of layer of BP which is nearest to metal surface is not destroyed on Al metal electrode unlike other metal electrodes. Therefore, we can predict SBH of all system from monolayer to four-layer BP.

In Fig. 13(a), the Fermi level is located between the conduction and valence bands and is closer to the VBM, where the p-type Schottky barrier forms. The p-type Schottky barrier height of Φ_{Bp} = 0.79 eV appears. From Figure.13 (b) to Figure.13 (d) as multilayer of BP, we measured difference between E_F and band splitting of VB. In Fig.13 (b), Energy difference between E_F and splitting band of VB are 0.4 and 0.62 eV respectively and averaged value is 0.51eV. Energy difference between E_F and CBM is 0.52 eV. The VBM of bilayer BP-Al contact system is closer to the Fermi levels and forms *p*-type contact where the p-type Schottky barrier height of Φ_{Bp} = 0.51 eV appears. In Figure.13 (c), Energy difference between E_F and splitting band of VB are 0.1, 0.6, 0.9, respectively and averaged value is 0.53 eV. Energy difference between E_F and CBM is 0.49 eV. The n-type Schottky barrier (Φ_{Bn}) forms where the n-type Schottky barrier height of Φ_{Bn} = 0.49 eV. In Figure13 (d), Energy difference between E_F and splitting band of VB are 0.0, 0.51, 0.6 and 1.08 eV respectively and averaged value is 0.55 eV. Energy difference between E_F and CBM is 0.38 eV. The CBM is closer to the Fermi level than the VBM, an n-type Schottky barrier (Φ_{Bn}) forms. The n-type Schottky barrier height of Φ_{Bn} = 0.38 eV appears. BP transistors with Al contacts demonstrate p-type behavior is switched to n-type behavior, as can be seen in Figure 13(a) and Figure 13(d). The variation of the SBH and carrier type as function of thickness from monolayer to four-layer BP are illustrated in figure 14 (a)-(c). It can be seen from figure

14. (b) that the SBH continuously drops when the number of layer increases, with varying from monolayer BP to four-layer BP in all metal case. As shown in Figure14. (c), all samples with Ti contacts displayed n-type behavior. On the other hand the dominant carrier type is switched in Sc and Al case. These results indicate that layer by layer carrier type control of black phosphorene-metal contact.

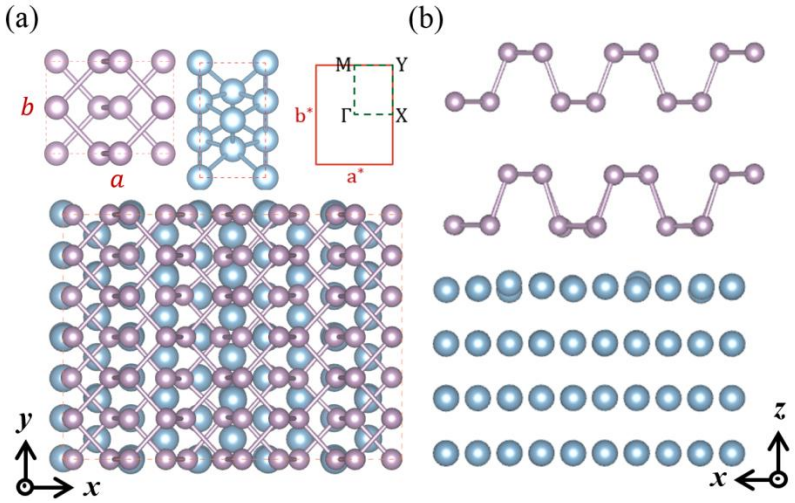

Figure 12. Interfacial structures of the most stable configuration for BP on metal surfaces. (a)Top views and (b) side view of double layer of BP on the Al (001) surface.

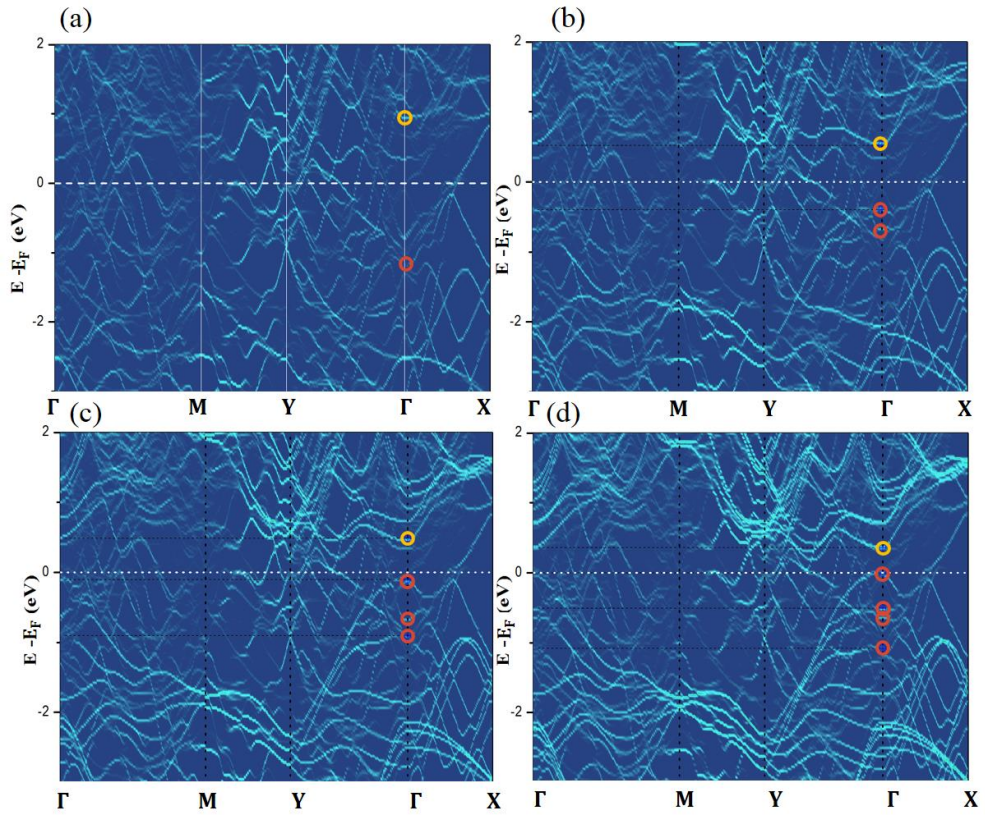

Figure 13. Calculated interfacial properties of BP on the Al metal surfaces. The unfolding band structure projected contributions from the wave function on the BP orbitals. The line width is proportional to the weight. The Fermi level is set at zero.

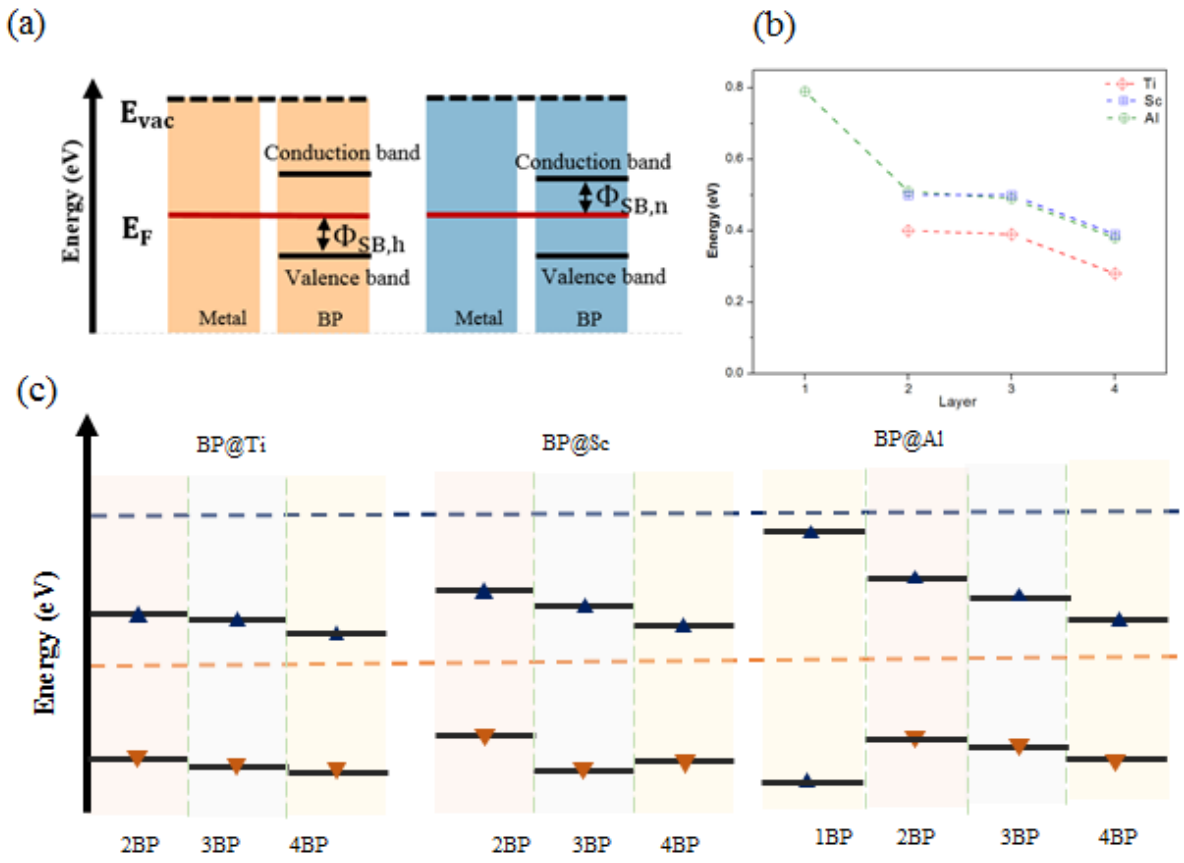

Figure 14. A schematic of the BP–metal interface contact.

V. SUMMARY

In summary, we have investigated the electronic properties of the BP-metal contacts by means of density functional theory calculations. We select Al, Ti, Sc metal as electrode and BP as channel. Due to the lattice mismatch between BP and metals, we carried out the supercell calculation. To directly observe the band structure of BP/metal contact, we use a band unfolding technique (BandUP). Our results show the contact metal and thickness of BP play a crucial role in changing a Schottky barrier height formed at BP/metal interface and controlling the dominant carrier type at BP/metal interface. According to our results, the layer by layer control allows significant tuning of the schottky barrier height as well as shows thickness dependence of dominant carrier type of BP-metal contact.

VI. Reference

[1] Hugh O.H.Churchill and Pablo Jarillo-Herrero, “Two-dimensional crystals: phosphorus joins the family.” *Nature Nanotech.* **9**, 330-331, (2014)

[2] Y.Du, C. Ouyang, S. Shi and M. Lei, “Ab initio studies on atomic and electronic structures of black phosphorus” *J. Appl. Phys.* **107**, 093718, (2010).

[3] H. Liu, Y. Du, Y. Deng, DY. Peide, “Semiconduction black phosphorus: systhesis, transport properties and electronic applications”, *Chem. Soc. Rev*. **44**, 2732-2743, (2015)

[4] L. Li , Y. Yu , Guo Jun Ye, Q. Ge , X. Ou , H. Wu , D. Feng , Xian Hui Chen and Yuanbo Zhang, “Black phosphorus field-effect transistors” *Nature Nanotechnology.* **9**, 372–377, (2014)

[5] S. Das, M. Dermarteau, and A. Roelofs, “Ambipolar phosphorene field effect transistor” *ACS Nano.* **8**, 11730-11738, (2014)

[6] Y. Du, H. Liu, Y. Deng, P.D. Ye, “Device perspective for Black Phosphorus field-effect transistors: contact resistance, ambipilar behavior, and scaling. *ACS Nano*. **8**, 10035-10042, (2014)

[7] M. Buscema, D.J. Groenendijk, S. I. Blanter, G. A. Steele, H. S. J. van der Zant, and A. Castellanos-Gomez, "Fast and Broadband Photoresponse of Few-Layer Black phosphorus Field-Effect Transistors" *Nano Lett*. **14(6)**, 3347-3352, (2014)

[8] J. Qiao, X. Kong, Z.Xin Hu, F. Yang and W.Ji, "High-mobility transport anisotropy and linear dichroism in few-layer black phosphorus" *Nature Communications*. **5,** 4475, (2014)

[9] Liu H, Neal AT, Zhu Z, Luo Z, Xu X, Tomanek D, Ye PD, "Phosphorene: an unexplored 2D semiconductor with a high hole mobility." *ACS NANO*. **8(4),** 4033-4041, (2014)

[10] H. Liu, A.T. Neal, Z. Zhu, D. Tomanek, P.D. Ye, "Phosphorene: a new 2D material with high carrier mobility"**,** ACS Nano, **8**, 4033-4041 (2014)

[11] Eugenie Samuel Reich, "Phosphorene excites materials scientists" *Nature.* **506**, 19, (2014)

[12] V. Tran, R. Soklaski, Y. Liang and L. Yang, "Layer-controlled band gap and anisotropic excitons in few-layer black phosphorus" *Phys.Rev.B.* **89**, 235319, (2014)

[13] H. Zhong, R. Quhe, Y. Wang, Z. Ni, M. Ye, Z. Song, Y. Pan, J. Yang, L. Yang, J. Shi, and J. Lu, "Interfacial Properties of Monolayer and Bilayer MoS_2 Contacts with Metals: Beyond the Energy Band Calculation" *Scientific Reports*. **6**, 21786, (2016)

[14] L.Huang, N. Huo, Y. Li, H. Chen, J. Yang, Z. Wei, J. Li, and S.S. Li "Electric-Field

Tunable Band offsets in Black Phosphorus and MoS_2 van der Waals p-n Heterostructure" *J. Phys. Chem. Lett*. **6(13)**, 2483-2488, (2015)

[15] S. Das, "Tunable transport gap in Phosphorene" *Nano Lett*. **14**, 5733-5739, (2014)

[16] Y. Pan, Y. Wang, M. Ye, R. Quhe, H. Zhong, Z. song, X. Peng, D. Yu, J, Yang, J, Shi, and J. Lu, "Monolayer Phosphorene-metal contacts" *Chem. Mater*. **28(7)**, 2100-2109, (2016)

[17] J.E. Padilha, A. Fazzio, and Antonio J.R. da Silva, "van der Waals Heterostructure of Phosphorene and Graphene: Tunning the Schottky Barrier and Doping by Electrostatic Gating" *Phys. Rev. Lett*. **114**, 006803, (2015)

[18] B. Liu, L.J. Wu, Y.Q. Zhao, L.Z. Wang, and M.Q. Cai, "Tuning the Schottky barrier height of the Pd - MoS_2 contact by different strains" *Phys. Chem. Chem. Phys*. **17**, 27088-27093, (2015)

[19] Y. Deng, Z. Luo, N.J. Conrad, H. Liu, Y. Gong, S. Najmaei, P.M. Ajayan, j. Lou, X. Xu, and P.D. Ye, "Black Phosphorus-Monolayer $\mathbf{MoS_2}$ van der Waals Heterojunction p-n Diode" *ACS Nano*. **8**, 8292-8299, (2014)

[20] A. Kahn, N. Koch, and W. Gao, "Electronic structure and electrical properties of interfaces between metals and $\boldsymbol{\pi}$ – conjugated molecular films" *Polymer Physics,* **41,** 2529-2548, (2003)

[21] W. Chen, E.J.G Santosm W. Zhu, E. Kaxiras, and Z. Zhang, "Tuning the Electronic and Chemical Properties of Monolayer MoS_2 Adsorbed on Transition Metal Substrates" *Nano Lett*. **13(2)**, 509-514, (2013)

[22] J. Kang, W. Liu, D. Sarkar, D. Jena, and K. Banerjee, "Computational Study of Metal Contacts to Monolayer Transition-Metal Dichalcogenide Semicondutors" *Phys. Rev. X*. **4**, 031005, (2014)

[23] K. Gong, L. Zhang, W. Li, and H. Guo, "Electrical contacts to monolayer black phosphorus: A first principle investigation" *Phys. Rev. B*. **90**, 125441, (2014)

[24] A. Chanana, and S. Mahapatra, "First principles study of metal contacts to monolayer black phosphorus" *J.Appl.phys.* **116**, 204302, (2014)

[25] Y. jiao, A. Hellman, Y. Fang, S. Gao, and M. kall, "Schottky barrier formation and band bending revealed by first-principles calculations" *Scientific Reports*. **5**, 11374, (2015)

[26] S. Zhu, Y. Ni, J. Liu, and K. Yao, "The study of interaction and charge transfer at black phosphorus-metal interfaces" *J. Phys. D: Appl. Phys.* **48**. 445101, (2015)

[27] Winfried Mönch. Semiconductor Surfaces and Interfaces, Springer

[28] F. Leonard and J. Tersoff, "Role of Fermi-Level Pinning in Nanotube Schottky Diodes" *Phys. Rev. Lett*. **84**. 4693, (2000)

[29] Chemical bonding and Fermi Level Pinng at metal-Semiconductor Interfaces, *Phys. Rev. Lett.* **84**, 6078-6081, (2000)

[30] W. E. Spicer, P. W. Chye, P. R. Skeath, C. Y. Su, and I. Lindau, "New and unified model for Schottky barrier and III–V insulator interface states formation" *J. Vac. Sci. Technol.* **16**, 1422, (1979)

[31] F. J. Himpsel, G. Hollinger, and R. A. Pollak, "Determination of the Fermi-level pinning position at Si (111) surfaces" *Phys. Rev. B.* **28**, 7014, (1983)

[32] P. Hohenberg and W. Kohn, "Inhomogeneous Electron Gas" *Phys. Rev.* **136**, B864, (1964)

[33] W. Kohn and L. J. Sham, "Self-Consistent Equations Including Exchange and Correlation Effect" *Phys. Rev.* **140**, A1133, (1965)

[34] D. M. Ceperley and B. J. Alder, "Ground State of the Electron Gas by a Stochastic Method." *Phys. Rev. Lett.* **45**, 566, (1980)

[35] S. H. Vosko, L. Wilk, and M. Nusair, "Accurate spin-depent electron liquid correlation energies for local spin density calculations: a critical analysis." *Can. J. Phys*. **58**, 1200, (1980)

[36] J. P. Perdew, Y. Wang, "Accurate and simple analytic representation of the electron-gas correlation energy." *Phys. Rev. B.* **23**, 13244, (1992)

[37] A. D. Becke, *J. Chem. Phys*. **98,** 5648, (1993)

[38] J. P. Perdew, J. A. Chevary, S. H. Vosko, K. A. Jackson, M. R. Pederson, D. J. Singh, and C. Fiolhais, *Phys. Rev. B.* **46,** 6671, (1992)

[39] J. P. Perdew, K. Burke, and M. Ernzerholf, Phys. *Rev. Lett*. **77,** 3865, (1996)

[40] J. P. Perdew and Y. Wang, "Accurate and simple analyric representation of the electron-gas correlation energy" *Phys. Rev. B.* **45**, 13244, (1992)

[41] G.Kresse and J. Hafner , *Phys. Rev. B*. **49,** 14251, (1994)

[42] G. Kresse and J. Furthmuller, *Phys. Rev. B*. **54**, 11169, (1996)

[43] Kittel, Charles. *Introduction To Solid State Physics,* JohnWiley&SonsInc, (2004)

[44] H. J. Monkhorst, J. D. Pack, "Special Points for Brillouin-Zone Integrations" *Phys. Rev. B.* **13**, 5188-5192. **(**1976)

[45] P. V. C. Medeiros, S. Stafstrom, and J. Bjork "Effects of extrinsic and intrinsic pertubatons on the eletronic structure of graphene: Retaining an effective primitive cell band structure by band unfolding" *Phys. Rev. B.* **89**, 041407(R), (2014)

[46] W. Ku, T. Berlijn, and C. C. Lee, "Unfolding First-Principles Band Structures" *Phys. Rev. Lett.* **104**, 216401, (2010)

[47] A. N. Rudenko, M. I. Katsnelson, "Quasiparticle band structure and tight-binding model

for single- and bilayer black phosphorus" *Phys. Rev. B.* **89** 201408(R), (2014)

[48] W. Kohn, L. J. Sham, "Self-Consistent Equations Including Exchange and Correlation Effects" *Phys. Rev*. A. **140**, 1133-1138, (1965)

[49] G. Kresse, J. Furthmüller, "Efficiency of ab-initio Total Energy Calculations for Metals and Semiconductors Using a Plane-Wave Basis Set" *Comp. Mater. Sci.* **6**, 15-50, **(**1996)

[50] J. P. Perdew, K. Burke, M. Ernzerhof, "Generalized Gradient Approximation Made Simple" *Phys. Rev. Lett*. **77**, 3865-3868, (1996)

[51] W. Kohn, L. J. Sham, "Self-Consistent Equations Including Exchange and Correlation Effects" *Phys. Rev*. A. **140**, 1133-1138, (1965)

[52] G. H. Olsen "Interfacial lattice mismatch effects in III–V compounds", *Journal of Crystal Growth*. **31**, 223-239, (1975)

[53] Y. Cai, G. Zhang, and Y. -W. Zhang, "Layer-dependent Band Alignment and Work Function of Few-Layer Phosphorene" *Sci. Rep*. **4**, 6677 (2014)

[54] P. E. Blöchl, "Projector Augmented-Wave Method" *Phys. Rev. B.* **50**, 17953-17979, **(**1994)

[55] M. Z. Rahman, C. W. Kwong, K. Davey and S. Z. Qiao "2D phosphorene as a water splitting photocatalyst: fundamentals to applications" *Energy Environ. Sci*. **9**, 709-728, (2016)

요 약 문

흑린은 인 원자로 이루어진 2차원 물질 포스포린이 적층된 구조로 박막으로서의 응용 가능성과 적절한 밴드갭과 우수한 전자이동도를 가지고 있어 새로운 이차원 반도체 소자에 대한 연구가 활발하게 진행중이다. 소자를 구현하기 위해서는 반도체와 금속에서 발생하는 접촉 저항과 전자전달특성을 조절하는 것이 중요하다

본 연구는 band unfolding 기술을 이용하여 포스포린과 금속 접합의 전자 구조를 구하고 layer by layer 조절을 함으로써 금속과 반도체의 접합부에서 생기는 전위 장벽 높이와 다수캐리어의 종류를 제어할 수 있음을 보였다.

핵심어: 제일원리계산, 포스포린, 전계 효과, 트랜지스터, 접촉 저항, 전위 장벽